DEFLECTION OF CORONAL MASS EJECTION IN THE INTERPLANETARY MEDIUM

YUMING WANG, CHENGLONG SHEN, S. WANG and PINZHONG YE
School of Earth and Space Sci., Univ. of Sci. and Tech. of China
(e-mail: ymwang@ustc.edu.cn)

(Received 7 January 2004; accepted 18 May 2004)

Abstract. A solar coronal mass ejection (CME) is a large-scale eruption of plasma and magnetic fields from the Sun. It is believed to be the main source of strong interplanetary disturbances that may cause intense geomagnetic storms. However, not all front-side halo CMEs can encounter the Earth and produce geomagnetic storms. The longitude distribution of the Earth-encountered front-side halo CMEs (EFHCMEs) has not only an east–west (E–W) asymmetry (Wang *et al.*, 2002), but also depends on the EFHCMEs' transit speeds from the Sun to 1 AU. The faster the EFH-CMEs are, the more westward does their distribution shift, and as a whole, the distribution shifts to the west. Combining the observational results and a simple kinetic analysis, we believe that such E–W asymmetry appearing in the source longitude distribution is due to the deflection of CMEs' propagation in the interplanetary medium. Under the effect of the Parker spiral magnetic field, a fast CME will be blocked by the background solar wind ahead and deflected to the east, whereas a slow CME will be pushed by the following background solar wind and deflected to the west. The deflection angle may be estimated according to the CMEs' transit speed by using a kinetic model. It is shown that slow CMEs can be deflected more easily than fast ones. This is consistent with the observational results obtained by Zhang *et al.* (2003), that all four Earth-encountered limb CMEs originated from the east. On the other hand, since the most of the EFHCMEs are fast events, the range of the longitude distribution given by the theoretical model is E40°,W70°, which is well consistent with the observational results ($E40°$, $W75°$).

1. Introduction

A solar coronal mass ejection (CME) is a large-scale eruption of the plasma and magnetic fields from the Sun (e.g., Howard *et al.*, 1982, 1985; Hundhausen, 1988, 1993; Gosling, 1990, 1996; Webb *et al.*, 2000; St. Cyr *et al.*, 2000; Gopalswamy *et al.*, 2000). Generally, a typical CME injects roughly 10^{23}maxwells of magnetic flux and 10^{13}kg of plasma into interplanetary space (Gosling, 1990; Webb *et al.*, 1994). CMEs are believed to be the main sources of the strong interplanetary disturbances that cause many moderate to intense geomagnetic storms (e.g., Sheeley *et al.*, 1985; Gosling *et al.*, 1991; Webb *et al.*, 2000; Wang *et al.*, 2003).

Since CMEs may be approximated as axial directed symmetrical structures, the front-side halo CMEs are thought to be directed towards the Earth and most likely causing geomagnetic storms (Howard *et al.*, 1982). However, not all front-side halo CMEs have geoeffectiveness. Webb *et al.* (2000) analyzed the relationship between

Solar Physics **222:** 329–343, 2004.

halo CMEs, magnetic clouds (MCs), and geomagnetic storms, and suggested that the halo CMEs associated with solar activity within 0.5 $R_\odot$ of Sun center appear to be excellent indicators of increased geoactivity 3–5 days later. By analysis of 36 Earth-directed halo CMEs, Cane *et al.* (2000) suggested that the locations of typical geoeffective solar events are in longitude $\lesssim 40°$ east and west. Gopalswamy *et al.* (2000) also found that CMEs originating near the central meridian with average longitude about 17° will not miss the Earth. All the studies above show that the Earth-encountered CMEs' sources concentrate near the central meridian and their distribution seems to be approximately symmetric in longitude.

To the contrary, recent results suggested that the solar source distribution of the geoeffective halo CMEs has east–west (E–W) asymmetry by statistically examining the LASCO (Large-Angle Spectroscopic Coronagraph on board the Solar and Heliospheric Observatory)-observed halo CMEs from March 1997 to 2000 (Wang *et al.*, 2002). The number of geoeffective halo CMEs originating from the west hemisphere is larger than that from the east by 57%, and such CMEs may be expected at $\sim$ W70° but cannot be beyond E40°. A similar asymmetry in the source longitude distribution was presented by Cane *et al.* (1988) for helium abundance enhancements, though the E–W asymmetry was not proposed definitely. Recently, Cane and Richardson (2003) further confirmed the results by analysis of a more complete sample of front-side halo CMEs. Moreover, in the identification of the solar sources of major geomagnetic storms between 1996 and 2000, Zhang *et al.* (2003) also obtained the same conclusion about such an E–W asymmetry.

E–W asymmetrical distribution has always been found in sunspots, solar flares, solar magnetic structures, etc. (e.g., Maunder, 1907; Bartsch, 1973; Heras *et al.*, 1990; Joshi, 1995; Meunier, 2003). However, these asymmetries are different from our results because our results are obtained by investigating only the halo CMEs reaching the Earth. For all front-side halo CMEs, the distribution does not appear E–W asymmetric (Wang *et al.*, 2002).

The E–W asymmetry in previous studies implies that the west halo CMEs more likely encounter the Earth and therefore cause geomagnetic storms. Wang *et al.* (2002) and Zhang *et al.* (2003) suggested that the Parker spiral interplanetary magnetic fields (Parker, 1963) deflect CMEs when they propagate in the interplanetary medium. CMEs will move outward along a curved line but not a straight line, and form an asymmetric distribution source. Cane and Richardson (2003) raised another possible explanation that some CMEs preferentially occur to the east of the active region in terms of differential rotation. To reveal the nature of this asymmetry and further find whether it has other new characteristics, we investigate the definite Earth-encountered front-side halo CMEs (EFHCMEs) during 1996 – 2002 again by using the Cane and Richardson (2003) sample, and give an approximate theoretical analysis. The observations are described in the next section. The results are presented in Section 3. In Section 4, a possible theoretical explanation is given. Finally, we conclude and summarize the paper in Section 5.

2. Observations

The primary observations of CMEs are from the LASCO/SOHO, EIT/SOHO and GOES satellites. They are used to select the front-side halo CMEs. The halo CMEs defined here are the CMEs with a span angle larger than 100°. On the other hand, the primary interplanetary observations, which are used to identify the interplanetary counterparts of the CMEs, namely ICMEs, are from the ACE and Wind spacecraft (e.g., Hirschberg, Bame, and Robbins, 1972; Burlaga *et al.*, 1981; Farrugia *et al.*, 1993; Richardson and Cane, 1995; Neugebauer and Goldstein, 1997). Here, to make our results more believable, we do not use our own sample of front-side halo CMEs (Wang *et al.*, 2002), but use the Cane and Richardson (2003) sample listed in Table I of their paper. In their list, some events are ambiguous and some events result from multiple CMEs (as marked by 'i' and 'j' in their table). These ambiguous events and multi-source events are excluded to make the facts more clear. In all, 69 Earth-encountered front-side halo CMEs are selected for analysis. Table I lists some parameters of these EFHCMEs. The CMEs' average transit speeds (V_t) from the Sun to the Earth are estimated by the CMEs' first appearance in C2/LASCO and their arrival at the Earth. CME source locations on the solar surface are mainly identified by SOHO observations. Identifying the source location is often difficult because a CME is a large-scale phenomenon and its onset may extend over a significant fraction of the solar disk (Harrison, 1986; Plunkett *et al.*, 2001). Here, following the Wang *et al.* (2002) and Zhou, Wang, and Coa (2003) methods, we define the source locations: the initial sites of CMEs, from which the CMEs were triggered, and identify the initial sites by viewing LASCO/EIT movies as well as *Yohkoh* SXT images. Details can be found in the two papers cited above. Certainly, an error in locating the CME's initial site is inevitable. An error of 10° is estimated empirically. For a case study, such an error may be a fatal flaw. In a statistical study, its influence should be reduced.

3. Results

An index, δ_L, defined by

$$\delta_L = \frac{L_W + L_E}{2} \ , \tag{1}$$

where L_W and L_E are the longitudes of the most west EFHCME and the most east EFHCME respectively, is used to evaluate the asymmetry. This index shows the shift of the source distribution from the central meridian.

The solar sources of all of the EFHCMEs are scattered in a large range from $E40°$ to $W75°$ approximately (as seen in Figure 1), which is consistent with our previous results (Wang *et al.*, 2002). The asymmetry index $\delta_L = 18.5°$ indicates that the source distribution shifts to the west. Generally the west halo CMEs meet the Earth more easily than the east ones.

TABLE I

List of the Earth-encountered front-side halo CMEs during 1996–2002.

CMEs			ICMEs		T^a	$V_t{}^b$	CMEs			ICMEs		T^a	$V_t{}^b$
date	time	location	date	time	hours	km s^{-1}	date	time	location	date	time	hours	km s^{-1}
			1996				05/10	2006	S26W10	05/13	1700	69.0	603.9
12/19	1630	S14W09	12/23	1700	96.5	431.8	05/13	1226	S22W41	05/16	2300	82.5	505.1
			1997				05/20	1450	S37W45	05/23	1000	67.0	621.9
01/06	1510	S18E06	01/10	0400	85.0	490.2	07/07	1026	N23W41	07/11	0200	87.5	476.2
02/07	0030	S22W45	02/10	0200	73.5	566.9	07/11	1327	N18E36	07/13	1600	50.5	825.1
04/07	1427	S25E16	04/11	0600	87.5	476.2	07/14	1054	N17W02	07/15	1900	32.0	1302.1
05/12	0630	N21W08	05/15	0900	74.5	559.3	07/23	0530	N05E20	07/27	0200	92.5	450.5
05/21	2100	N07W12	05/26	1600	115.0	362.3	08/09	1630	N20E12	08/12	0500	60.5	688.7
07/30	0445	N25W20	08/03	1300	104.0	400.6	09/05	0554	N22E10	09/08	1800	84.0	496.0
08/30	0130	N32E11	09/03	1300	107.5	387.6	10/02	2026	S10W01	10/05	1300	64.5	646.0
09/17	2028	N45W15	09/21	2100	96.5	431.8	10/09	2350	N02W06	10/13	0800	80.0	520.8
09/28	0108	N30E10	10/01	1600	87.0	478.9	10/25	0826	N20W66	10/28	2100	84.5	493.1
10/06	1528	S54E19	10/10	2200	102.5	406.5	11/08	2306	N09W75	11/10	1000	35.0	1190.5
10/23	1126	N25E05	10/27	0000	84.5	493.1				2001			
11/04	0610	S18W30	11/07	0400	70.0	595.2	02/28	1450	S17W05	03/04	0400	85.0	490.2
11/19	1227	N20E11	11/22	1500	74.5	559.3	03/16	0350	S08W09	03/19	1700	85.0	490.2
12/06	1027	N40W20	12/10	1800	103.5	402.6	03/29	1026	N15W12	04/01	0400	65.5	636.1
			1998				04/10	0530	S23W09	04/11	2200	40.5	1028.8
01/02	2328	N32W11	01/07	0100	97.5	427.4	04/11	1331	S22W27	04/13	0900	43.5	957.9
01/25	1526	N24E25	01/29	1400	94.5	440.9	04/26	1230	N23W02	04/28	1400	49.5	841.8
02/14	0655	S25E27	02/17	1000	75.0	555.6	08/14	1601	N37E17	08/17	2000	76.0	548.2
02/28	1248	S24W02	03/04	1300	96.0	434.0	09/28	0854	N12E18	10/01	0800	71.0	586.9
04/29	1658	S15E19	05/02	0500	60.0	694.4	09/29	1154	N14E02	10/02	1200	72.0	578.7
10/15	1004	N15W21	10/19	0400	90.0	463.0	10/09	1130	S30E10	10/12	0200	62.5	666.7
11/04	0418	N20W02	11/07	2200	89.5	465.5	10/19	1650	N16W30	10/22	0000	55.0	757.6
11/05	2044	N20W23	11/08	1900	70.5	591.0	10/22	1826	S18E18	10/27	0000	101.5	410.5
11/09	1818	N20W02	11/13	0200	79.5	524.1	10/25	1526	S18W20	10/29	2200	102.5	406.5
			1999				11/04	1635	N06W18	11/06	2100	52.5	793.7
04/13	0330	N20W02	04/16	1800	86.5	481.7	11/22	2330	S17W35	11/24	1400	38.5	1082.3
08/17	1331	N20E34	08/20	2300	81.5	511.2				2002			
09/20	0606	S18E01	09/22	1900	61.0	683.1	02/12	1506	N12E38	02/15	1000	67.0	621.9
10/18	0026	S20E05	10/21	0800	79.5	524.1	03/15	2306	S07W08	03/19	0500	78.0	534.2
			2000				04/17	0826	S13W12	04/20	0000	63.5	656.2
01/18	1754	S16E04	01/22	1700	95.0	438.6	05/22	0326	S15W70	05/23	2000	40.5	1028.8
02/08	0930	N27E15	02/11	1600	78.5	530.8	07/29	1145	S12W16	08/02	0400	88.0	473.5
02/10	0230	N25E02	02/12	1200	57.5	724.6	08/16	1230	S10E19	08/19	1200	71.5	582.8
02/17	2006	S23W15	02/21	0600	82.0	508.1	09/05	1654	N12E27	09/08	0400	59.0	706.2
04/04	1632	N16W60	04/07	0700	62.5	666.7	09/17	0754	S10W33	09/19	2000	60.0	694.4

[a]The transit time of the CME from the first appearance in C2/LASCO to the arrival at 1 AU.
[b]The average transit speed of the CME in the interplanetary medium.

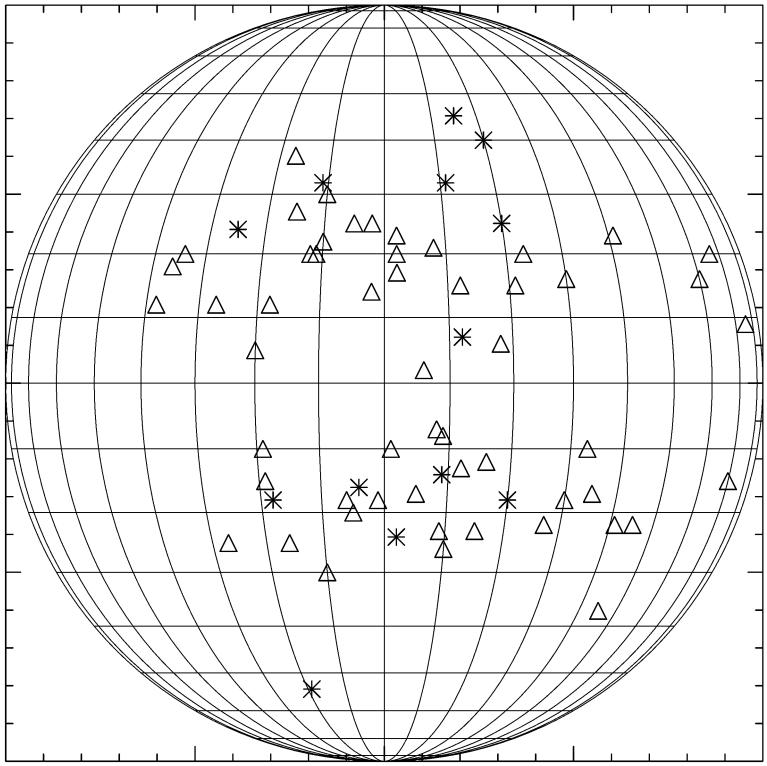

Figure 1. The source distribution of all the EFHCMEs on the solar disk. Symbols △ and ∗ denote the events with the average transit speed (V_t) larger and smaller than the average solar wind speed ($V_{au} \approx 450$ km s^{-1}), respectively.

Further, we investigate whether there is a relationship between the distribution and the EFHCME's average transit speeds (V_t) from the Sun to 1 AU. We chose the speed of V_s as a borderline to divide the EFHCMEs into two groups: fast ones with $V_t \geq V_s$ and slow ones with $V_t < V_s$. The solar wind speed along the Sun-Earth line at 1 AU is $V_{au} \sim 450$ km s^{-1} on average during 1996–2002. Therefore, let $V_s = V_{au}$, there are 56 fast events and 13 slow events as marked by △ and ∗ respectively in Figure 1. It is reasonable that a majority ($56/69 \sim 81\%$) of the EFHCMEs propagate faster than the background solar wind. The E–W asymmetry of the fast EFHCMEs is significantly the same as that of the entire EFHCMEs due to the domination of fast events. In contrast, for the slow EFHCMEs, the source distribution shifts slightly from the central meridian. The longitude range of the source region of the slow EFHCMEs is E30°, W25° approximately, much narrower than that of the fast ones. The index $\delta_L = -2.5°$ approaches zero, and the E–W asymmetry is largely weakened.

We suppose that such an E–W asymmetry is indeed related to the average transit speeds (V_t) of EFHCMEs. Let V_s vary from $\sim$ 400–540 km s^{-1}, we obtain the

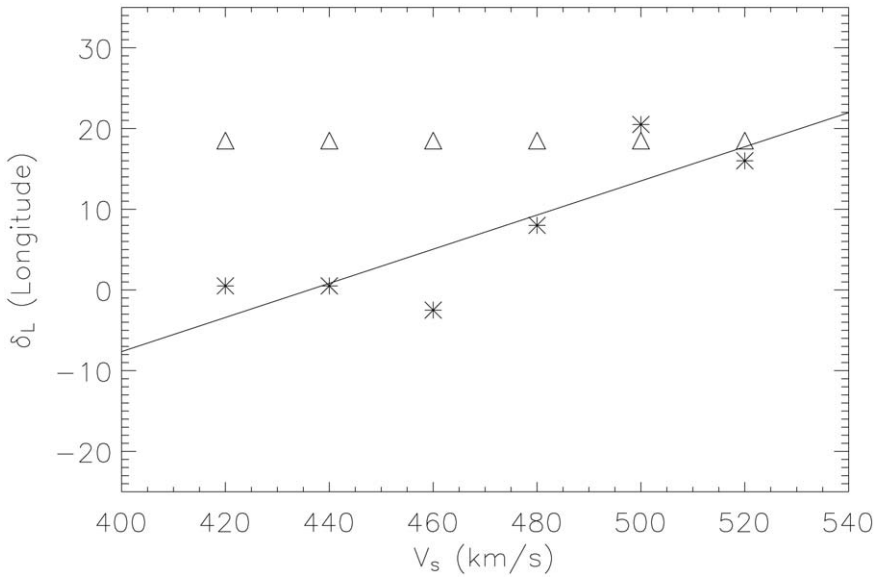

Figure 2. The E–W asymmetry index δ_L versus the speed V_s. Symbols $\triangle$ and $*$ indicate δ_L versus V_s for the fast ($V_t \geq V_s$) and slow ($V_t < V_s$) EFHCMEs, respectively. The *straight line* is the linear fit of slow events.

relationships between the δ_L and V_s as shown in Figure 2. Since the majority of EFHCMEs were fast ones, the longitude range of fast ones does not change and the index δ_L is always 18.5°. To the contrary, as V_s increases, the source distribution of slow ones tends to shift westward more and more. By using a linear fit, we obtain a slope of 0.21. It can be seen that for the very slow EFHCMEs the distribution shifts to the east, and generally the faster the EFHCMEs are, the more westward their distribution.

Figure 3 shows the distributions of EFHCMEs' transit speeds to 1 AU. The upper panel presents the transit speed histogram for the east events. The speeds are 350 km s^{-1} to 850 km s^{-1}. The lower panel presents the histogram for the west events. The speeds are scattered in a large range from 350 km s^{-1} to 1350 km s^{-1}. Compared to the upper panel, for the events with transit speeds below about 900 km s^{-1}, the distribution for west events is similar to that of east events. Beyond 900 km s^{-1}, the two distributions are totally different. The very large speed events only come from the west. This means that a fast, especially very fast, ICME observed near the Earth originates from the west on the solar disk.

Assuming that CMEs move along radial directions at the beginning, the above results of E–W asymmetry imply that CMEs will be deflected from the radial direction when they propagate in the interplanetary medium. Fast CMEs will deviate from radial to the east, whereas slow CMEs will deviate from radial to the west. We believe that the most likely explanation is that the propagation of a CME is influenced by the Parker spiral interplanetary magnetic field as described by

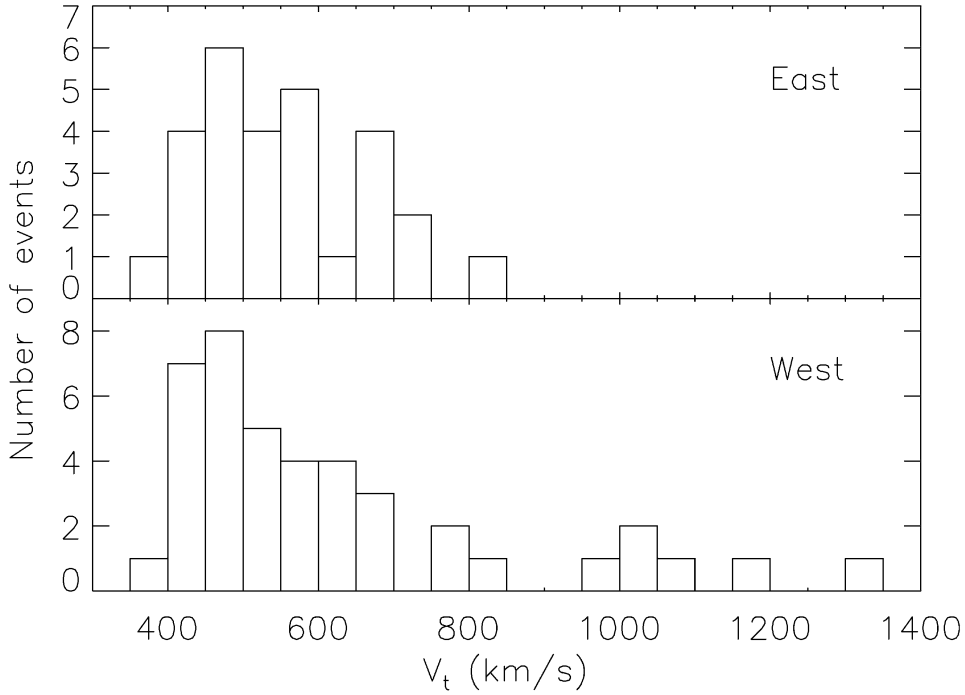

Figure 3. The histograms showing the distributions of the EFHCMEs' average transit speed.

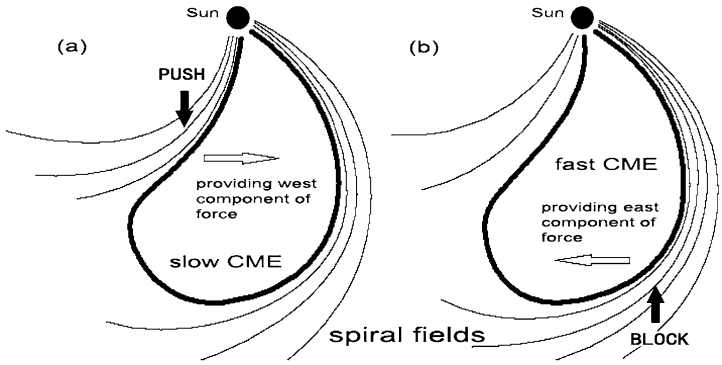

Figure 4. Schematic pictures of (a) slow and (b) fast CME propagation in the interplanetary medium.

the schematic pictures shown in Figure 4. Commonly, it is considered that the interplanetary magnetic field is frozen in the solar wind plasma. A spiral field is therefore formed due to the drag by radial outflows. When a CME moves slower than the background solar wind, the following flow pushes the CME which causes an enhancement of the total pressure behind roughly, which provides a force with a westward component to make the CME deflect to the west (Figure 4(a)). In contrast, when a CME moves faster than the background solar wind, the leading flow blocks the CME that causes an enhancement of the total pressure ahead roughly,

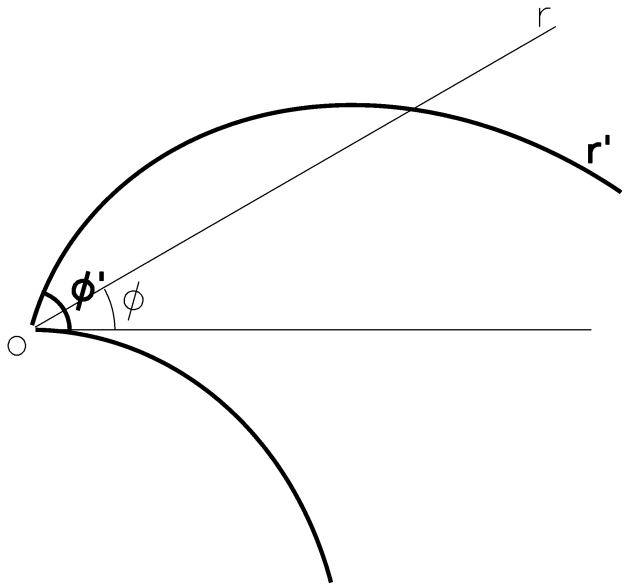

Figure 5. The coordinates of inertial frame (r, ϕ) and outflow frame (r', ϕ').

which provides a force with an eastward component to make the CME deflect to the east (Figure 4(b)). So a fast ICME observed near the Earth tends to originate from the west on the solar surface, and the faster the EFHCMEs are, the more westward does their distribution shift. Since the observed EFHCMEs mostly propagate faster than the background solar wind, the longitude distribution shifts westward as a whole.

Four cases of limb CMEs, which struck the Earth and caused major geomagnetic storms (refer to Table IV in the Zhang *et al.* (2003) paper), illuminate such deflections further. These four solar-terrestrial events were identified by Zhang *et al.* (2003) recently and they all originated from the east solar limb. Since the projection effect is small for limb events, we consider their observed projected speeds in LASCO to be real speeds. It is found that these four east-limb CMEs are all very slow with speeds of 247 km s^{-1}, 138 km s^{-1}, 233 km s^{-1}, and 173 km s^{-1}, respectively. According to the above supposition, these east-limb slow CMEs should be deflected to the west when they propagated in the interplanetary medium, and we therefore observed them near the Earth.

4. Kinetic Interpretation

A simple theoretical analysis is carried out here to support our point of view and obtain some primary properties of such a deflection of CMEs. The Parker spiral magnetic field is formed due to the drag by radial outflows and the rotation of the Sun (Parker, 1963). In an ecliptic plane (r, ϕ) image a series of outflows with

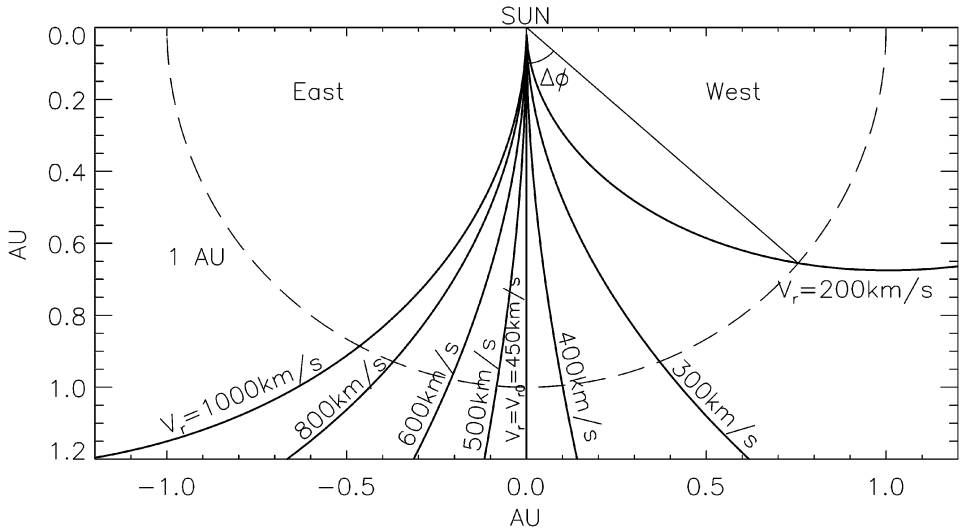

Figure 6. The configuration of the interplanetary background spiral magnetic field seen from radial outflow with various speed V_r. When $V_r = V_{r0}$, where V_{r0} is the speed of background solar wind, the spiral field line is presented as a straight line.

velocity $V_0 = (V_{r0},0) \approx (450,0)$ km s^{-1} (here, we will ignore the non-radial motion), the spiral field line can be described by

$$r = -\frac{V_{r0}}{\Omega}(\phi - \phi_0) \ , \tag{2}$$

where $\Omega \approx 2.7 \times 10^{-6}$ rad s^{-1} is the angular velocity of the Sun's rotation and ϕ_0 is the direction of the initial outflow, in terms of ideal MHD. The field line is spiral in an inertial frame, whereas it is a straight line seen from the outflows. So we can change the frame from (r, ϕ) to the outflow frame (r', ϕ'), in which the background spiral field is described as a straight line (Figure 5). The transform formulae are given by

$$\begin{cases} r' = \displaystyle\int_0^r \sqrt{1+\frac{\Omega^2}{V_{r0}^2}r^2}\mathrm{d}r = \frac{1}{2a_0}\left[r\sqrt{r^2+a_0^2}+a_0^2\ln(r+\sqrt{r^2+a_0^2})\right] - \frac{a_0}{2}\ln a_0 \\ \phi' = \phi + \dfrac{\Omega}{V_{r0}}r = \phi + \dfrac{r}{a_0} \ , \end{cases} \tag{3}$$

where $a_0 = V_{r0}/\Omega$.

For the outflows with various radial speeds, the configuration of the spiral field line dragged by it varies, but the form of the frame transform does not change. Given an arbitrary outflow with speed V_r, the transform from (r, ϕ) to the frame (r', ϕ') moving with the outflow may be written by just dropping the subscript '0' in Equations (3):

$$\begin{cases} r' = \dfrac{1}{2a}[r\sqrt{r^2+a^2} + a^2 \ln(r+\sqrt{r^2+a^2})] - \dfrac{a}{2}\ln a, \\ \phi' = \phi + \dfrac{r}{a} \end{cases} \tag{4}$$

where $a = V_r/\Omega$. Assuming the outflow is not influenced by the background magnetic field, the background spiral field line will be a curved line in the outflow frame (r', ϕ') if the speed V_r of the outflow is not equal to the background solar wind speed V_{r0}. Combining Equations (2) and (4), the background spiral field line is described by

$$\begin{cases} r' = \dfrac{1}{2a}[r\sqrt{r^2+a^2} + a^2 \ln(r+\sqrt{r^2+a^2})] - \dfrac{a}{2}\ln a, \\ \phi' = \left(\dfrac{1}{a} - \dfrac{1}{a_0}\right) r \end{cases} \tag{5}$$

in an outflow frame (r', ϕ').

The configurations of the background spiral field line in the frames with various radial outflows have been shown in Figure 6. In the frame of fast outflow, the field line deflects to the east, and in contrast, the field line deflects to the west in the frame of slow outflow. Therefore, if a CME with a radial speed $V_r \neq V_{r0}$ propagates along the field line, a deflection of the CME can be expected. The force making the CME deviate from the direction of radial is illustrated in Figure 4. This result is consistent with the observational result shown in Figure 2, which implies that the faster the EFHCMEs are, the more westward does their distribution shift. Figure 7 shows the deflection angle ($\Delta\phi$) of CMEs with various radial speeds in ecliptic plane at 1 AU. It should be noticed that a slow CME is the deflected more easily than a fast one. When V_r = 200 km s^{-1}, the deflection angle is about 50°. When V_r = 1800 km s^{-1}, the deflection angle is only $-30°$ approximately. A 90° deflection may be expected as long as the CME is slow enough. This means that the east-limb slow CMEs possibly encounter the Earth, which is consistent with the Zhang *et al.* (2003) result.

Statistical studies suggested that CMEs are typically 60° in angular extent (Howard *et al.*, 1985; Cane, 1988). So there is a range of source longitude, from which a CME with a given speed can encounter the Earth, though the deflection is inevitable. Let $\Theta = 60°$ denote the average span angle of CMEs in the ecliptic plane and φ denote the source longitude of CMEs. To ensure a CME does not miss the Earth, r' must be larger than 1 AU when $\phi' - (-\varphi) = \pm\Theta/2$ according to Equation (5). Considering the critical situation, we get:

$$\begin{cases} \dfrac{1}{2a}[r\sqrt{r^2+a^2} + a^2 \ln(r+\sqrt{r^2+a^2})] - \dfrac{a}{2}\ln a = 1 \text{ AU}, \\ \left(\dfrac{1}{a} - \dfrac{1}{a_0}\right) r + \varphi = \pm\dfrac{\Theta}{2} \end{cases} \tag{6}$$

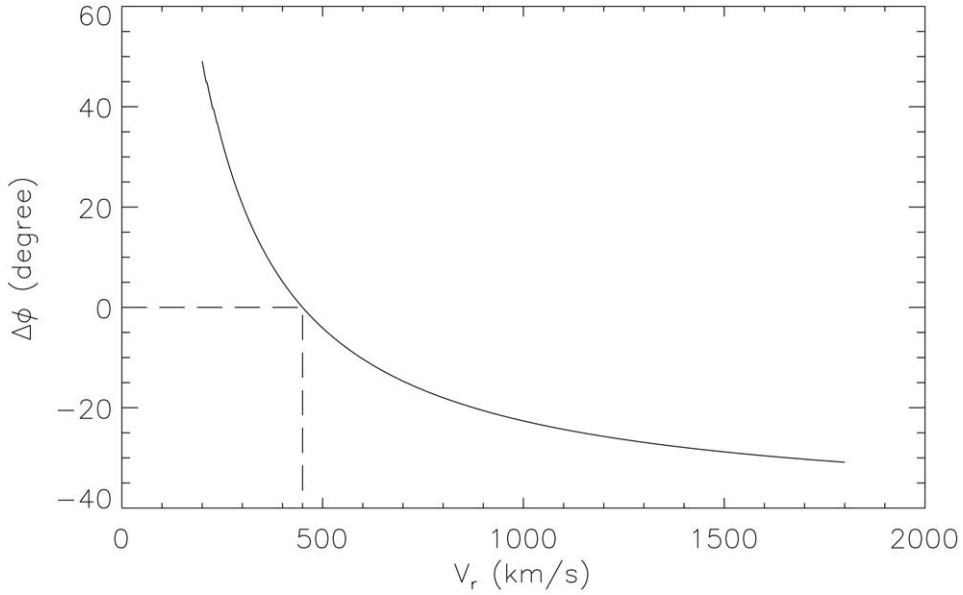

Figure 7. The deflection angle ($\Delta\phi$) in ecliptic plane at 1 AU versus the radial speed (V_r) of CMEs.

i.e.,

$$r\sqrt{r^2+a^2} - 2a = a^2 \ln \frac{a}{r+\sqrt{r^2+a^2}} \quad , \tag{7}$$

where $r = (\pm(\Theta/2) - \varphi)[a_0 a/(a_0 - a)]$. Using this formula, we can estimate the upper and lower limits of a EFHCME's transit speed $V_\pm$ (i.e., $a_\pm$) as a function of its source longitude.

The solid curves of $V_\pm$ shown in Figure 8 give the longitude range of EFHCMEs' sources in the case that the CMEs' average span angle is 60° in the ecliptic plane. Obviously, the transit speed range of the west CMEs is much wider than that of the east ones. The transit speed of a west CME may be any value larger than 260 km s^{-1} approximately, whereas that of a east CME cannot exceed 1100 km s^{-1}. This theoretical result is consistent with the observations shown in Figure 3 that the very large speed events only appear in the west, except that the estimated value of 1100 km s^{-1} is somewhat larger than the observational value of $\sim$900 km s^{-1}. Moreover, it can be seen that a west EFHCME will not originate beyond 70° if the average transit speed of CMEs does not exceed 1400 km s^{-1}, but an east EFHCME may occur near the solar limb as long as it is slow enough. This is why the limb Earth-encountered CMEs mentioned in the last paragraph of Section 3 all originated from the east. On the other hand, since almost all of CMEs are faster than 350 km s^{-1}, the source longitude range is [E40°, W70°] roughly, and the distribution therefore shifts to the west. This theoretical result is consistent with the observational result presented in last section that the solar sources of all EFHCMEs are scattered in a large range from E40° to W75°.

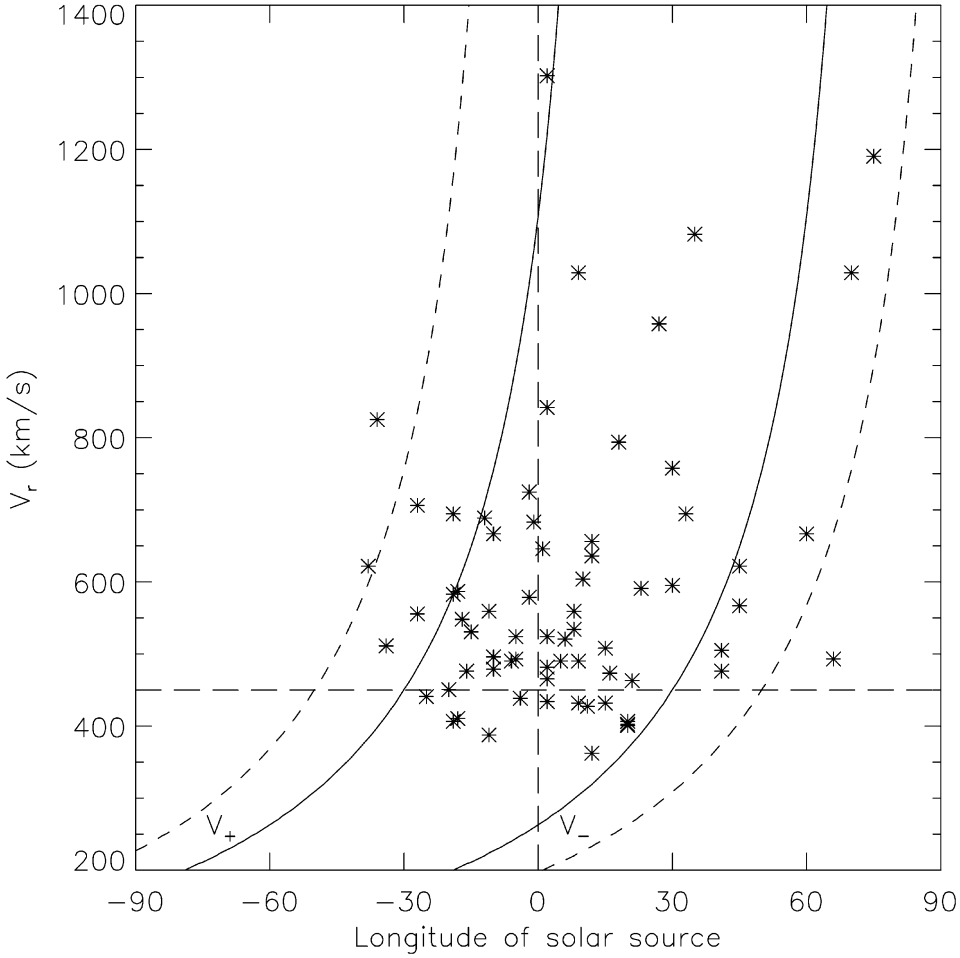

Figure 8. The longitude range of EFHCMEs' solar sources in the cases that the CMEs' average span angle is 60° (*solid curves*) and 100° (*dashed curves*) in longitude. The sample listed in Table I is marked by $*$.

To further compare the theory with the observations, we mark the sample listed in Table I in Figure 8 by the symbols $*$. 54 of all 69 (78%) EFHCMEs are located within the region between the two solid curves of $V_{\pm}$ in Figure 8. It should be noticed that all of the 15 EFHCMEs inconsistent with the theoretical results are fast events whose transit speeds are larger than the background solar wind speed and all of the slow EFHCMEs satisfy the theoretical condition. It seems that the theoretical analysis is more suitable for slow ones than fast ones. Why are there only some fast EFHCMEs not obeying the theoretical rule? In the process of reasoning, an implied assumption is that the background spiral magnetic field dragged by solar wind is fixed, i.e., a CME with arbitrary speed will move out along the background field line. For slow CMEs, their kinetic energy is relatively low, and the background

magnetic field therefore dominates. In this case, the above assumption is good. However, for fast CMEs, their kinetic energy is much higher. The background field is not dominant, and it will be deformed by fast CMEs' drag. Fast CMEs will not move strictly outward along the estimated field line. So some fast events are not consistent with this model.

In addition, the influence of CME's span angle (Θ) on the estimation is evident. In fact, much wider CMEs have been observed (McAllister *et al.*, 1996, e.g.). The dashed curves in Figure 8 present the case of $\Theta = 100°$. It is clear that the estimated source range at any transit speed is wider than that with span angle $\Theta = 60°$. For a wider CME coming from a given longitude, the likelihood to meet the Earth becomes larger. In this case, only 3 CMEs do not locate in the region between the two dashed curves.

The theoretical analysis described above is simple. An exact calculation of CMEs' deflection is not expected from it. But we can only use this simple theoretical model to describe the gross properties of the deflection of the CMEs' motion and explain why the source distribution of EFHCMEs is E–W asymmetrical. For a detailed and deep understanding CME propagation in the interplanetary medium the methods of dynamic analysis, e.g., MHD simulations, should be applied.

5. Conclusions and Summary

Based on the observational results and kinetic analysis, the following conclusions are obtained:

(1) A majority ($56/69 \approx 81\%$) of the EFHCMEs propagate faster than the background solar wind.

(2) The propagation of CMEs is influenced by the interplanetary spiral magnetic field. The fast CMEs will be deflected to the east, whereas the slow CMEs will be deflected to the west. The deflection angle can be roughly estimated according to the CME's transit speed.

(3) Slow CMEs can be deflected more easily than fast ones. A very slow east-limb CME may be expected to reach the Earth, but it is difficult to observe a west-limb CME itself near the Earth. The fact that four limb CMEs mentioned in the last paragraph of Section 3 all originated from the east supports this point.

(4) As a whole, the source distribution of all EFHCMEs is E–W asymmetric. It shifts to the west and includes all of the EFHCMEs located in the region of [E40°, W75°] because most of them are fast events.

(5) In detail, the source distribution is related to the transit speed of CMEs due to the deflection. The EFHCMEs faster than the background solar wind occurred within a wide longitude range from E40° to W75°, whereas the slow EFHCMEs only appeared in a narrow range from E30° to W25° approximately. Generally, the faster the EFHCMEs are, the more westward their distribution shifts. The very fast EFHCMEs prefer originating from the west.

In summary, we statistically study 69 EFHCMEs from 1996 to 2002, and find that the source distribution of them is E–W asymmetric which is related to the CMEs' transit speed from the Sun to 1 AU. Combining the observational results and the simple theoretical analysis, we believe such asymmetry is due to the deflection of CMEs' propagation in the interplanetary medium. These results are meaningful in the field of space weather. How to apply them to predict whether and when a CME will arrive at the Earth according to the observations of the Sun is worthy to be studied in a future work.

Acknowledgements

We acknowledge the use of the data from the SOHO, *Yohkoh*, GOES, ACE and Wind spacecraft. This work is supported by the Chinese Academy of Sciences (KZCX2-SW-136), the National Natural Science Foundation of China (40336052, 40336053), and the State Ministry of Science and Technology of China (G2000078405).

References

Bartsch, R.: 1973, *Solar Phys.* **30**, 93.
Burlage, L., Sittler, E., Mariani, F., and Schwenn, R.: 1981, *J. Geophys. Res.* **86**, 6673.
Cane, H. V.: 1988, *J. Geophys. Res.* **93**, 1.
Cane, H. V. and Richardson, I. G.: 2003, *J. Geophys. Res.* **108**, 1156.
Cane, H. V., Richardson, I. G., and St. Cyr, O. C.: 2000, *Geophys. Res. Lett.* **27**, 3591.
Farrugia, C. J., Burlaga, L. F., Osherovich, V. A., Richardson, I. G., Freeman, M. P., Lepping, R. P., and Lazarus, A. J.: 1993, *J. Geophys. Res.* **98**, 7621.
Gopalswamy, N., Lara, A., Lepping, R. P., Kaiser, M. L., Berdichevsky, D., and St. Cyr, O. C.: 2000, *Geophys. Res. Lett.* **27**, 145.
Gosling, J. T.: 1990, in C.T. Russel, E. R. Priest and L. C. Lee (eds.), *Coronal Mass Ejections and Magnetic Flux Ropes in Interplanetary Space. Physics of Magnetic Flux Ropes*, AGU Geophys. Mon. **58**, p. 343.
Gosling, J. T.: 1996, *Annu. Rev. Astron. Astrophys.* **34**, 35.
Gosling, J. T., McComas, D. J., Phillips, J. L., and Bame, S. J.: 1991, *J. Geophys. Res.* **96**, 731.
Harrison, R. A.: 1986, *Astron. Astrophys.* **162**, 283.
Heras, A. M., Sanahuja, B., Shea, M. A., and Smart, D. F.: 1990, *Solar Phys.* **126**, 371.
Hirschberg, J., Bame, S. J., and Robbins, E. E.: 1972, *Solar Phys.* **23**, 467.
Howard, R. A., Michels, D. J., Sheeley, Jr., N. R., and Koomen, M. J.: 1982, *Astrophys. J.* **263**, L101.
Howard, R. A., Sheeley, Jr., N. R., Koomen, M. J., and Michels, D. J.: 1985, *J. Geophys. Res.* **90**, 8173.
Hundhausen, A. J.: 1988, in V. Pizzo, T. E. Holzer, and D. G. Sime (eds.), *Proceedings of the Sixth International Solar Wind Conference*. Boulder, pp. 181–214.
Hundhausen, A. J.: 1993, *J. Geophys. Res.* **98**, 13177.
Joshi, A.: 1995, *Solar Phys.* **157**, 315.
Maunder, A. S. D.: 1907, *Monthly Notices Royal Astron. Soc.* **67**, 451.
McAllister, A. H., Dryer, M., McIntosh, P., Singer, H., and Weiss, L.: 1996, *J. Geophys. Res.* **101**, 13497.

Meunier, N.: 2003, *Astron. Astrophys.* **405**, 1107.
Neugebauer, M. and Goldstein, R.: 1997, in N. Crooker, J. A. Joselyn, and J. Feynman, J. (eds.), *Coronal Mass Ejections*. Washington D.C., pp. 245.
Parker, E. N.: 1963, *Interplanetary dynamical processes.* Wiley Interscience, New York.
Plunkett, S. P., Thompson, B. J., St. Cyr, O. C., and Howard, R. A.: 2001, *J. Atmospheric Terrest. Phys.* **63**, 389.
Richardson, I. G. and Cane, H. V.: 1995, *J. Geophys. Res.* **100**, 23397.
Sheeley, Jr., N. R., Howard, R. A., Koomen, M. J, Michels, D. J., Schwenn, R., Mulhauser, K. H., and Rosenbauer, H.: 1985, *J. Geophys. Res.* **90**, 163.
St. Cyr, O. C., Howard, R. A., Sheeley, Jr. N. R., Plunkett, S. P., Michels, D. J., Paswaters, S. E., Koomen, M. J., Simnett, G. M., Thompson, B. J., Gurman, J. B., Schwenn, R., Webb, D. F., Hildner, E., and Lamy, P. L.: 2000, *J. Geophys. Res.* **105**, 18169.
Wang, Y. M., Ye, P. Z., and Wang, S.: 2003, *J. Geophys. Res.* **108**, 1370.
Wang, Y. M., Ye, P. Z., Wang, S., Zhou, G. P., and Wang, J. X.: 2002, *J. Geophys. Res.* **107**, 1340.
Webb, D. F., Cliver, E. W., Crooker, N. U., St. Cyr, O. C., and Thompson, B. J.: 2000, *J. Geophys. Res.* **105**, 7491.
Webb, D. F., Forbes, T. G., Aurass, H., Chen, J., Martens, P., Rompolt, B., Rusin, V., Martin, S. F., and Gaizauskas, V.: 1994, *Solar Phys.* **153**, 73.
Zhang, J., Dere, K. P., Howard, R. A., and Bothmer, V.: 2003, *Astrophys. J.* **582**, 520.
Zhou, G., Wang, J., and Cao, Z.: 2003, *Astron. Astrophys.* **397**, 1057.